Catena 211 (2022) 105987

Contents lists available at ScienceDirect

Catena

journal homepage: www.elsevier.com/locate/catena

Modeling seasonal soil moisture dynamics in gley soils in relation to groundwater table oscillations in eastern Croatia

Vedran Krevh [a], Vilim Filipović [a,*], Lana Filipović [a], Valentina Mateković [a], Dragutin Petošić [a], Ivan Mustać [a], Gabrijel Ondrašek [a], Igor Bogunović [a], Zoran Kovač [b], Paulo Pereira [c], Salini Sasidharan [d], Hailong He [e], Jannis Groh [f,g], Christine Stumpp [h], Giuseppe Brunetti [h]

[a] University of Zagreb, Faculty of Agriculture, 10000 Zagreb, Croatia
[b] University of Zagreb Faculty of Mining, Geology and Petroleum Engineering, 10000 Zagreb, Croatia
[c] Environmental Management Laboratory, Mykolas Romeris University, LT-08303 Vilnius, Lithuania Paulo
[d] Department of Environmental Sciences, University of California Riverside, Riverside, CA 92521, USA
[e] College of Natural Resources and Environment, Northwest A&F University, No.3 Taicheng Road, Yangling 712100, PR China
[f] Working Group "Hydropedology", Research Area 1 "Landscape Functioning", Leibniz Centre for Agricultural Landscape Research (ZALF), Müncheberg 15374, Germany
[g] IBG-3: Agrosphere, Institute of Bio- and Geoscience, Forschungszentrum Jülich GmbH, Jülich 52428, Germany
[h] Institute for Soil Physics and Rural Water Management, University of Natural Resources and Life Sciences, Vienna 1190, Austria

ARTICLE INFO

Keywords:
Vadose zone
Groundwater level
Zero-tension lysimeters
Capillary fringe
Unsaturated porous media
Numerical simulations
HYDRUS

ABSTRACT

This study aims to explain complex vadose zone hydrology of fine-textured (gley) agricultural soils influenced by a shallow and dynamic groundwater (GW) levels. The field site was located in the Biđ field (Eastern Croatia), where a detailed soil survey was performed. The simulations included a three-year period (2016–2018) at four locations. Soil hydraulic parameters (SHP) were estimated based on variables determined in the laboratory, while soil water flow was monitored using in-field zero-tension lysimeters. Piezometers were installed and used to monitor daily oscillations of groundwater levels (average depth to GW 2.2 m), while data from nearby Sava River was monitored. Unsaturated flow and water regime assessment was performed using HYDRUS-1D numerical modeling. Additional SHP optimization of van Genuchten-Mualem parameters (α and n) was performed using Shuffled Complex Evolution algorithm (SCE). The autocorrelation analysis was used to detect patterns in the precipitation, GW, and river level time series, while the Mutual Information (MI) was used to estimate the codependence of the processes in unsaturated zone and the main hydrological events. The model successfully (R^2 0.72 – 0.94) reproduced measured lysimeters outflows. The outflows from lysimeters were connected to precipitation patterns, transpiration intensity, and soil moisture content influenced by the shallow water table. Comparable MI values obtained for precipitation, GW, and river level suggest a concurrent role of these parameters in the unsaturated flow dynamics. The relationship between upward flux/water storage change into the domain, and transpiration/growth stages, suggests a strong connection between the water fluxes and the root water uptake. Results confirm the importance of GW for the agricultural production due to the major influence on upper soil layer moisture.

1. Introduction

The expansion of the world population and irrigated agriculture is identified as a major global risk to the sustainable development of human society (Mekonnen and Hoekstra, 2016; Vörösmarty et al., 2000). The groundwater (GW) exploitation due to increasing demand for drinking and agriculture negatively affects water bodies globally (Li et al., 2020; Wada et al., 2014). However, water resource management in arid and semi-arid regions with low precipitation, high evapotranspiration (ET) rate, and depleting GW is a challenging task that needs to be addressed in the future (Safavi et al., 2010). In addition, seasonal surface water levels of rivers, lakes, and wetlands are the main cause of complex and dynamic GW flows (Winter, 1999). Expansion of knowledge on surface and groundwater interaction has a significant impact on

* Corresponding author.
E-mail address: vfilipovic@agr.hr (V. Filipović).

https://doi.org/10.1016/j.catena.2021.105987
Received 19 May 2021; Received in revised form 11 November 2021; Accepted 23 December 2021
0341-8162/© 2021 Elsevier B.V. All rights reserved.

the utilization of water resources and its management (Bailey et al., 2016), water legislative, environmental protection, GW and surface water quality, river flow requirement to maintain aquatic ecological balance (Yang et al., 2020), or when evaluating water balance in the soil–plant-atmosphere continuum (Han et al., 2015).

Gaining a fundamental knowledge of the interaction between changing climatic conditions, irrigation practices, water quality (e.g., salinity and nutrients), shallow GW regime, and their effects on root water uptake is essential for sustainable agriculture (Askri et al., 2014). Numerous regions with shallow aquifers provide a continuous supply of water to the root zone due to capillary rise; thus, it is an essential water resource (Chen and Hu, 2004) as it provides additional water source for transpiration processes of agricultural crops (Karimov et al., 2014). GW level affects crop yield and explains large parts of yield variations (Nosetto et al., 2009). Root zone moisture has a vital role in ecological and hydrological processes, including evapotranspiration, infiltration, runoff, and erosion, and has the pivotal importance for terrestrial arable ecosystems (Zheng et al., 2015). Furthermore, soil water content is crucial for provisioning nutrients to crops, as well as for regulating and supporting ecosystem services (e.g., soil formation, soil fertility) (Adhikari and Hartemink, 2016; Cao et al., 2018; Vereecken et al., 2016). Climate change scenarios will additionally modify the spatial and temporal availability of soil water, as it will increase the frequency and duration of extreme events, like droughts (Fischer and Knutti, 2014), thus affecting the quantity and quality of aquifer recharge (Wu et al., 2019). Therefore, future agro-ecosystem productivity (e.g., crop yield) is expected to respond to changes in weather (short-term) and climate (long-term), because it will alter the crop water balance components such as soil water content, ET and drainage (Yang et al., 2016). Although only representing 0.05% of global freshwater sources, soil water supports all terrestrial life; therefore, its precise quantification and knowledge on its evolution in the soil-plant-atmosphere nexus is of major importance (Robinson et al., 2019).

In addition, soil water content depends on soil texture, organic matter content, bulk density, and soil structure, and it is related to the effective field water capacity, which can be derived from the soil water retention function (Vereecken et al., 2010). A poorly understood component of the soil–plant atmosphere continuum is the role of shallow GW as an in-situ driver for available soil water content within the root zone and its effects on yield variability, as well as how soil texture and inter-annual precipitation variability influences this relationship (Ayars et al., 2006). The interactions between soil texture, GW table depth, and meteorological conditions during vegetation period are important for assessing the available water within the root zone. Recent global analyses of water table data indicate that GW may be within or near the root zone in 22 to 32% of the terrestrial ecosystems (Fan et al., 2013). Improving our understanding and modeling of the interactions between shallow GW and root zone, as well as crop productivity, is identified as a critical research priority (Fan, 2015). It was found that in agricultural areas with a coarse soil texture where GW table depth is characterized as deep (>3 m), crops performed poorly with respect to the yields. Moreover, modeling results confirmed that beneficial impacts of shallow GW are more common than negative impacts (i.e., anaerobic stress) under the studied conditions, and that the optimal GW table depth is shallower in coarser soils (Zipper et al., 2015). Thus, there is an optimal range of GW level, where strong correlations between GW and land surface energy fluxes exist (Kollet and Maxwell, 2008), which largely depends on the soil properties of the vadose zone (Groh et al., 2016).

Water flow modeling within the vadose zone has a great importance in the up-to-date approach for the protection of water resources and sustainable agricultural production (Šimůnek and Bradford, 2008). One of the most frequently used vadose zone models is the HYDRUS-1D model, which solves the Richards equation for water movement (Šimůnek et al., 2016). Numerical HYDRUS-1D model is often used for the estimation of hydraulic soil and solute transport properties, soil water content, water infiltration and recharge (Bethune et al., 2008; Gogolev, 2002; Groh et al., 2018; Jiménez-Martínez et al., 2009; Mattern and Vanclooster, 2010; Stumpp et al., 2012). In addition, the effects of several combinations of soil type and various root distributions in vegetated shallow GW environment can be simulated (Grimaldi et al., 2015). Accurate estimations of GW recharge are essential for effective management of GW resources and, where possible, including long-term data about climate, irrigation practices, and soil physical parameters with the numerical approach is preferred (Lu et al., 2011). HYDRUS-1D model was used to simulate soil moisture in the root zone soil layer (*P. euphratica)* to investigate the contribution of GW to the root zone (Zhu et al., 2009). Similarly, HYDRUS-1D was used to investigate the effect of shallow water table on water use of the winter wheat (*Triticum aestivum* L.), where numerical simulations have shown that the contribution of the GW to ET increases with a rising water table and decreases with increasing irrigation applications (Karimov et al., 2014). HYDRUS-1D model was additionally found to be useful for analysing complex flow processes in fine-textured soil subject to transient water-table boundary conditions in Italy (Ventrella et al., 2000).

As changes in climate over space and time affect crucial aspects of subsurface hydrology, surface-GW interactions, and water quality (Green, 2016), regional and global surface water and GW resources are consequently affected as well (Zhang, 2015). The soil in the vadose zone has a regulating function, as well as the storage function, for governing the water balance that provides sufficient water to plants during droughts and alleviates or eliminates plant water stress (Nestroy, 2008). The function of soil moisture memory effect buffers drought impacts by still constituting soil structure from past wet conditions in its future state (Martínez-De La Torre and Miguez-Macho, 2019). However, it can also delay drought recovery with a carry-over of drought effect from one to another growing season; thus, long-term monitoring of soil water components is key for accurate water balance estimates (Groh et al., 2020).

Although performing numerical simulations is standard when estimating vadose zone processes (Šimůnek et al., 2016), seasonal variations, and GW table influence are often neglected, mostly due to the absence of measurements. However, the moisture content in the upper soil layers or in the rhizosphere of soils with shallow groundwater table (e.g., gley soils) can be directly influenced and thus need to be considered in the modeling. This is particularly true for fine-textured soils, where water retention properties extent the influence of the rising GW table (e.g., Groh et al., 2016), but it also largely depends on hydraulic model used for the simulation of soil hydraulic properties (Soylu et al., 2011). A similar conclusion was presented in a study where HYDRUS 2D/3D was used to assess water flow and nitrate fluxes in silty clay soils with a shallow GW table in eastern Croatia (Filipović et al., 2013). In the same study, the objective was to estimate the efficiency of the zero-tension plate lysimeters for 4 years. The two-dimensional simulation illustrated the potential influence of zero-tensiometer lysimeter plate on water flow and solute transport with the shallow GW table. However, detailed research regarding the interactions between precipitation and GW, including the surface water (river) effect was not evaluated.

In the presented study, on the same experimental site, HYDRUS-1D was coupled with detailed experimental data to quantify the effect of GW oscillations on moisture in the upper soil layers. The general aim was to determine water regime of unsaturated soil zone at selected locations in Eastern Croatia of fine-textured (gley soils), with respect to the seasonal variation of GW level, seasonal precipitation distribution, and a nearby river water level. The objectives were to i) improve the prediction of in-field leachate fluxes using HYDRUS-1D numerical modeling, and to ii) describe the interaction between local precipitation, vadose zone hydrological processes, and shallow GW dynamics, while including the influence of river level. This study was conducted by combining field monitoring using installed piezometers and zero-tension lysimeters, with laboratory measurements of soil physical parameters, and numerical simulations.

2. Data and methods

2.1. Experimental site and soil properties

The research area is located at Biđ field in Eastern Croatia. The area is geographically located between 18° 25′ to 18° 33′ E and 45° 07′ to 45° 11′ N. Climate data was collected from a nearby meteorological station at Gradište (45° 09′ N and 18°42′ E). Long-term (1986–2018) average annual cumulative precipitation and average annual temperature were 686.4 mm and 11.81 °C, respectively (Figure S1.). The period studied covered 2016, 2017 and 2018, with annual precipitation values of 745.9, 580.4 and 851.8 mm, respectively. The study was performed at four selected locations, representing the dominant soil types in that area. Soil types were classified as follows: Luvic Stagnic Phaeozem Siltic (Horizons: Ap-Bt-Bg-C) locations L1 and L2 and Haplic Gleysol Calcaric Eutric Siltic (Horizons: Ap-Bg-Cr-Cg) location L3 and L4. Soils at selected locations are strongly affected by GW level and, as such, can be classified in the Gleysols Reference Group according to IUSS (2015).

To measure the bulk density and the soil hydraulic properties at L1 - L4 locations, undisturbed soil samples (100 cm^3) were taken from the first two soil horizons (depths specified in Table 1). The saturated hydraulic conductivities (K_s) were measured using the constant head method (Klute and Dirksen, 1986). The saturated water content (θ_s) was measured using a saturation pan, and the points of the soil water content of the soil water retention curve (SWRC) were measured using a pressure plate apparatus (Dane and Hopmans, 2002) with applied pressure heads of 33, 625 and 1500 kPa. The particle size distribution was determined using the combination of sieving and sedimentation procedure, according to (Gee and Or, 2002). The measured basic physical soil properties are presented in Table 1.

During the research period, field crops were cultivated at selected locations with the application of standard agrotechnical measures (tillage and fertilization), typical for the conventional agricultural production in the region. Field crops cultivated during the research period were: oat (Avena sativa L., location 1), spelt (Triticum spelta L., location 2), winter barley (Hordeum vulgare L., location L3), soybean (Glycine max L., locations L1 and L2) and rapeseed (Brassica napus L., location L1 and L3). Zero-tension lysimeters (round, ∅50 cm, height 5 cm) were installed at the four selected locations (L1 - L4). At each location, the lysimeters were installed in pairs, altogether eight lysimeters were installed. A vertical trench was excavated to the depth of 2 m with an unearthed horizontal slot at a depth of 50 cm. The installation depth was selected, assuming high GW levels, implementation of usual agricultural practices (tillage), and effective root zone. A round lysimeter plate, filled with disturbed material (soil from that horizon), was inserted into the slot in order to leave the soil profile above the lysimeter plate undisturbed. To prevent small particles from being washed out with the leachate, a PVC net was applied on the lysimeter plate surface. Outflow pipes were installed and connected to soil water containers placed at the edge of the field to allow easy access. Leachate was monitored according to significant precipitation events throughout the year.

The daily GW levels were monitored using four water level measuring devices that were installed inside the four (4 m b.g.l.) piezometers (Orphimedes-OTT Hydrometry), located at the near proximity of installed lysimeters (2016 onward, all locations were equipped for daily measurements). The GW levels were monitored during 2004 – 2016period manually every ten days (Figure S2). PVC pipes (4 cm diameter) with a 40 cm perforated screen at the bottom was installed at the selected four locations in a borehole. The screen was covered with a fiber mesh and filled with a silica sand layer to prevent clogging. Additionally, a bentonite seal was used to fill the space between the soil and PVC to prevent the water from precipitation events to flow along the outer side of the tube and affect water level measurements. Sava River water levels were monitored by Croatian Waters Institute and the National hydrology program, available at: https://hidro.dhz.hr (last access: October 1, 2021.). Daily recorded groundwater oscillations (average of 2.2 m b.g.l.) during 2016–2018 (average distance between the piezometers of 7.3 km) and Sava River water level (recording station was located by an average distance of 11.25 km from piezometers) are presented in Fig. 1.

2.2. Water flow modeling and model validation

Water flow was simulated using the HYDRUS-1D program package (Šimůnek et al., 2016). For the simulation of water flow in a one-dimensional profile, Richards equation for variably saturated porous medium was used:

$$\frac{\partial\theta}{\partial t} = \frac{\partial}{\partial z}K\left(\frac{\partial h}{\partial z}+1\right) - S \tag{1}$$

where θ is volumetric soil water content [cm^3 cm^{-3}], h is pressure head [cm], K is hydraulic conductivity of unsaturated soil [cm day^{-1}], z is gravitational head [cm], t is time [day], and S is a sink term for root water uptake [day^{-1}].

Soil hydraulic functions were described using the van Genuchten-Mualem single porosity model (van Genuchten, 1980):

Table 1
Soil texture, saturated water content, soil bulk density, hydraulic conductivity, and water retention at selected pressure points, measured at four locations (L1 – L4) at Biđ experimental field, eastern Croatia.

Location	Depth (cm)	Sand %	Silt %	Clay %	Saturated water content (cm^3 cm^{-3})	Soil bulk density (g cm^{-3})	Saturated hydraulic conductivity (cm day^{-1})	Soil water content (cm^3 cm^{-3}) at pressure (kPa):		
								33	625	1500
L1	0–40	13	65	22	0.38	1.59	11	0.34	0.22	0.20
	40–75	4	63	33	0.37	1.57	15	0.34	0.22	0.20
	75–105	14	54	32	Not measured					
	105–200	5	69	26						
L2	0–30	9	67	24	0.36	1.56	17	0.33	0.17	0.16
	30–75	2	61	37	0.40	1.55	12	0.39	0.31	0.28
	75–130	8	72	20	Not measured					
	130–200	13	69	18						
L3	0–25	3	56	41	0.43	1.47	12	0.41	0.32	0.29
	25–80	2	57	41	0.41	1.46	10	0.35	0.22	0.20
	80–110	4	64	32	Not measured					
	110–200	5	69	26						
L4	0–30	5	54	41	0.42	1.37	12	0.39	0.28	0.22
	30–70	3	54	43	0.41	1.55	14	0.37	0.27	0.21
	70–150	3	54	43	Not measured					
	150–200	3	54	43						

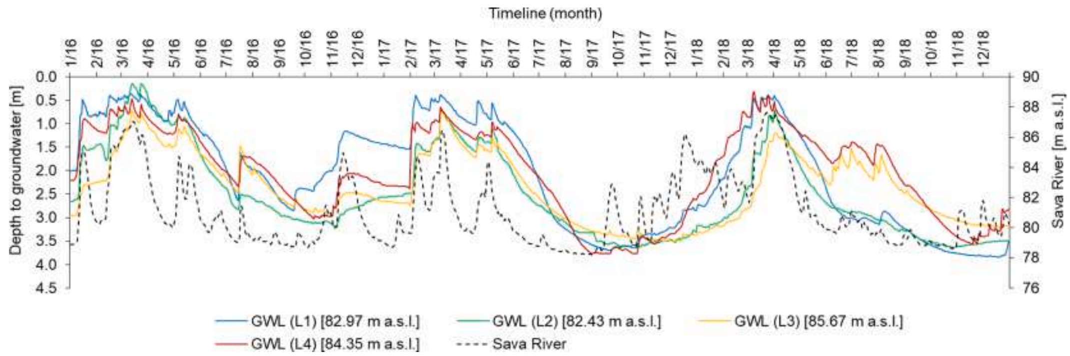

Fig. 1. Groundwater levels (GWL, presented as depth from the soil surface) at locations L1 - L4 at Biđ experimental field (eastern Croatia), presented with the nearby Sava River levels during 2016–2018.

$$\theta(h) = \theta_r + \frac{\theta_s - \theta_r}{(1 + |\alpha h|^n)^m} \text{ for h} < 0 \tag{2}$$

$$\theta(h) = \theta_s forh \geq 0 \tag{3}$$

$$K(h) = K_s S_e^l \left[1 - (1 - S_e^{\frac{1}{m}})^m\right]^2 (1-(1 - S_e^{\frac{1}{m}})^{m})^{2} \tag{4}$$

$$S_e = \frac{\theta - \theta_r}{\theta_s - \theta_r} \tag{5}$$

$$m = 1 - \frac{1}{n}; \text{n} > 1 \tag{6}$$

where $\theta(h)$ is volumetric water content [cm^3 cm^{-3}], $K(h)$ is hydraulic conductivity of unsaturated soil at water pressure head of h [cm], θ_r is residual soil–water content [cm^3 cm^{-3}], θ_s is water content in saturated soil [cm^3 cm^{-3}], S_e is the effective saturation, K_s is the saturated hydraulic conductivity of the soil [cm day^{-1}], α is the inverse of air-entry value (bubbling pressure), n is the dimensionless soil pore size distribution index, m is the dimensionless optimization coefficient, and l is the pore connectivity parameter [-].

For the first two depths, residual water content (θ_r) and empirical retention curve shape parameters (α and n) were initially estimated from parameters in Table 1, using the ROSETTA module (Schaap et al., 2001) embedded in HYDRUS-1D. For the following two depths, the same module was employed, using only soil texture from the soil survey (Table 1.) as an input, to generate remaining SHPs (θ_s, θ_r, K_s, α and n). Pore connectivity parameter (l), was set to 0.5 as found valid for most soil types (Mualem, 1976). After the first run of the simulations, during the model calibration, θ_r, α and n were optimized using Shuffled Complex Evolution (SCE) algorithm in R package SoilHyP (Dettmann, 2020). The SCE approach (Duan et al., 1993) is method of global optimization that is used for a number of hydrological problems (Groh et al., 2018; Ries et al., 2015; Vrugt et al., 2003). Relatively flat terrain allows assuming one-dimensional flow in the vertical direction, for which HYDRUS-1D was used. Three sets of simulations (SIM1, SIM2 & SIM3) were performed. In the first set of simulations (SIM1), a two-layered soil profile of 50 cm depth was assumed to mimic the soil system at experimental locations where lysimeters were installed (L1 - L4). These simulations allowed model validation based on the measured water outflow collected from the installed lysimeters. At the top boundary, atmospheric conditions with surface run-off, allowing precipitation and ET were assumed, while seepage face boundary condition with a specified pressure head (0 cm) was assumed for the bottom to mimic conditions for drainage measured by the zero-tension lysimeters. In the second set of simulations (SIM2), the profile was extended to 2 m depth. The material distribution was set according to Table 1. As in the first set, an atmospheric condition was applied at the top, while the bottom boundary was described by a variable pressure head conditions, which represented an oscillating water table (measured daily data). Initial conditions were defined as hydrostatic pressure head distribution, with the set value of the pressure head at the bottom (measured in the field on piezometers). For precise water balance calculations SIM2 was used. The third set of simulations (SIM3) was identical to SIM2, but had free drainage applied at the bottom boundary to investigate the influence of GW on actual ET processes and to demonstrate the difference in actual ET when no GW is present. The simulations were carried out for 2016 – 2018 (1096 days), which was taken as a representative for our study, and 2016 being the first year with the daily GW level recordings at all four investigated locations. The similar annual GW pattern was recorded during the long-term monitoring period (2004 – 2015, Figure S2). In all simulations (SIM1, SIM2 & SIM3) crop water uptake was assumed. For all crops, the root density distribution was set as value 1 at the top, and value 0.3 at the bottom of the root zone (following recommendation by Filipović et al., 2013 used the same site). The model of (Feddes et al., 1978) was used for root water uptake rates evaluation, which is assigned according to the pressure potential (h) of the soil water. Primarily, a plant-dependent, optimum uptake range exists between the two h values while the uptake rate decreases linearly to zero when h is above or below this range. These values were taken from the HYDRUS database for the corresponding crops at the sites. ET rates were calculated on a daily basis with the HYDRUS-1D model using the Penman-Monteith equation (Monteith, 1981) based on a combination of climatic parameters with crop growth parameters for each location (crop height, albedo, leaf area index (LAI) and root depth) (Breuer et al., 2003). A simplified LAI approach was used, assuming a linear increase of LAI until its peak at beginning of its late growth stage, given by FAO (Allen et al., 1998), following a linear decrease of 50% until harvest. Based on the output data of the simulations, water storage change (WSC) was calculated as:

$WSC = I - E - T + BF$ (7)where I is cumulative infiltration into the soil, E is cumulative evaporation from the soil surface, T is cumulative root water uptake (plant transpiration) and BF is cumulative net flux across the bottom boundary (-/+; out of the domain/into the domain).

Model validation was carried out with the coefficient of determination (R^2), the root-mean-square error (RMSE), and the Nash–Sutcliffe model efficiency coefficient (NSE).

$$R^2 = \left[\frac{\sum_{i=1}^{N}(O_i - \overline{O})(P_i - \overline{P})}{\left[\sum_{i=1}^{N}(O_i - \overline{O})^2\right]^{0,5}\left[\sum_{i=1}^{N}(P_i - \overline{P})^2\right]^{0,5}}\right] \tag{8}$$

$$RMSE = \sqrt{\frac{\sum_{i=1}^{N}(O_i - P_i)^2}{N}} \tag{9}$$

$$NSE = 1 - \frac{\sum_{i=1}^{N}(O_i - P_i)^2}{\sum_{i=1}^{N}(O_i - \overline{O})^2} \tag{10}$$

where O_i is observation, P_i is prediction, $\bar{O}$ is average observation and $\overline{P}$

is average prediction, while the N is the sample size.

2.3. Autocorrelation analysis and Mutual Information

The autocorrelation analysis was used to detect patterns in the precipitation, groundwater, and river level time series. The correlogram condenses the autocorrelation analysis results, and gives a qualitative idea of the "memory effect" in the hydrological time series. In general, a correlogram with a gentle slope suggests data series persistence, while a rapid decrease indicates the random nature of values.

The Mutual Information (MI) was used to estimate the codependence of the unsaturated zone behavior and the main hydrological quantities. In particular, the informational correspondence between the simulated time series of pressure head and soil volumetric water content at two different depths [$z = (-20, -50$ cm)], and the precipitation, groundwater level, and river level, was calculated. MI between two random variables X and Y is defined as:

$$I(X,Y) = \sum_{x\in X}\sum_{y\in Y} p(x,y)log_2\frac{p(x,y)}{p(x)p(y)} \quad (11)$$

where $p(x, y)$ is the joint probability of X and Y, and $p(x)$ and $p(y)$ are their marginal probability. Similarly, the MI can be calculated as the difference between the sum of the entropies of X and Y minus the joint entropy of X and Y:

$$I(X,Y) = H(X) + H(Y) - H(X,Y) \quad (12)$$

where $H(X)$ and $H(X, Y)$ are the Shannon and the joint entropy, respectively, defined as:

$$H(X) = -\sum_{x\in X} p(x_i)log_2 p(x_i) \quad (13)$$

$$H(X,Y) = -\sum_{x\in X}\sum_{y\in Y} p(x_i,y_i)log_2 p(x_i,y_i) \quad (14)$$

MI quantifies the amount of information that one variable reveals about another and thus the strength of their codependence. If the mutual information is zero, the two variables are independent, while high values correspond to stronger dependence. However, since the value of MI depends on the absolute magnitude of the joint entropy of the two selected variables, it is not appropriate to use MI for relative comparison. To avoid this problem, Normalized Mutual Information is used instead (Loritz et al., 2018; Michaels et al., 1998):

$$NMI(X,Y) = \frac{I(X,Y)}{max[H(X),H(Y)]} \quad (15)$$

The main advantage of using MI against traditional correlation functions is that the former makes no assumptions on the codependence of variables. However, while the covariance involved in the correlation analysis can be directly calculated from the data, the MI requires the knowledge of the probability density function of the variable considered. The estimation of the probability density function is prone to multiple problems, especially when dealing with hydrological time series:

Zero effect: precipitation records often contain a large number of days without any precipitation (zero values), which can bias the estimation of the MI. To circumvent this problem, nonzero and zero values are hereby handled separately in the process of entropy estimation (Chapman, 1986; Gong et al., 2014).

Optimal Bin Width: The selection of bin width is extremely important for the calculation of the probability distribution. Too small bin widths can lead to a histogram that is a too rough approximation of the underlying distribution, while large bin widths may result in a histogram that is too smooth compared to the true probability density function. In this work, the upper bound of the bin width was calculated by using the oversmoothed bandwidth rule (Gentle et al., 2012). To account for the observation error, the bin width is selected to be larger than the precision of the measurement. In particular, a precision of 0.01 cm^3 cm^{-3} and 2 cm was considered for the water content and pressure head, respectively, while an error of 0.2 mm day^{1-1}, 2 cm, and 5 cm, was set for the precipitation, groundwater level, and river level.

3. Results & discussion

3.1. Water flow and model validation

Cumulative values of leachate from zero-tension lysimeters and simulated values using HYDRUS-1D (SIM1) are presented in Fig. 2. Simulations were performed during the period of 2016 – 2018, for four lysimeter locations. The amounts of leachate measured were mostly connected with the increased soil moisture, low root water uptake, evaporation and climatic patterns (e.g., precipitation). Increasing ET rates and lower precipitation during the spring and summer time (Fig. 2), substantially lowered the amount of leachate. As previously found, the amount of leachate depends on the precipitation events and transpiration intensity (e.g., Filipović et al., 2013) while in the areas with shallow groundwater table, like here presented, the capillary rise might have significant importance for the crop growth (Gribovszki et al., 2010; Han et al., 2015). HYDRUS-1D was successfully validated using the lysimeter outflows at four selected locations (L1 - L4). The comparison of simulated and observed data showed satisfying results (R^2 0.72 – 0.94, Fig. 2). The standard deviation in annual drainage among the locations was 1, 2.1 and 2.5 cm for 2016, 2017 and 2018 respectively, which is rather small, and corresponds to the similar texture and soil hydraulic properties among locations (Tables 1 & 2). The NSE values for L1 – L4 averaged 0.84, −0.51 and 0.74 for 2016, 2017 and 2018 respectively. NSE values, as a performance evaluation tool, can range from $-\infty$ to 1, and are usually considered as a good fit if values are > 0.5 (Moriasi et al., 2007). Low NSE values for 2017 are connected to the low number of observation points caused by the lower than average precipitation (580.4 mm) and consequently to low amount of outflow at investigated locations.

These type of zero-tension lysimeters are often used because of low cost in acquisition and maintenance (e.g., Filipović et al., 2013; Westerhoff, White, & Rawlinson, 2018), as well for installation procedure which leaves soil above undisturbed and allow agricultural practices, e.g., tillage (Filipović et al., 2016). Here, modeling was performed using the HYDRUS-1D, as using the collected data (i.e., outflows from zero-tension lysimeter) can only serve for model validation of soil water flux at a specific soil depth. New lysimeter techniques are now available which can mimic upward directed water flow, which would be important, especially at sites with a shallow groundwater table and high dynamic capillary rise (Groh et al., 2020; Pütz et al., 2018). Such high precision lysimeter system can even be used when soil tillage is done with large agricultural machines at the field (Klammler and Fank, 2014). However, such high precision lysimeter are costly and infrastructurally intensive, making them suitable for long-term observation, e.g., for lysimeter networks (e.g., SOILCan, Pütz et al., 2016). Also, at sites with large local heterogeneity, for short observation period and influence of water flow dynamics (Coquet et al., 2005; Filipović et al., 2013, 2014) zero-tension or wick lysimeters plates are a feasible measurement system to provide data on soil water fluxes.

The model performance criteria for each location was achieved by the optimization based on the model performance and the SCE approach (Dettmann, 2020) which was identified as effective for this case. The final set of soil hydraulic parameters employed in the modeling study are presented in Table 2. This set of simulations (SIM1) used the collected water from zero-tension lysimeter data and can only be used for model validation of soil water flux at a specific soil depth while SIM2 was used for the precise water balance calculation.

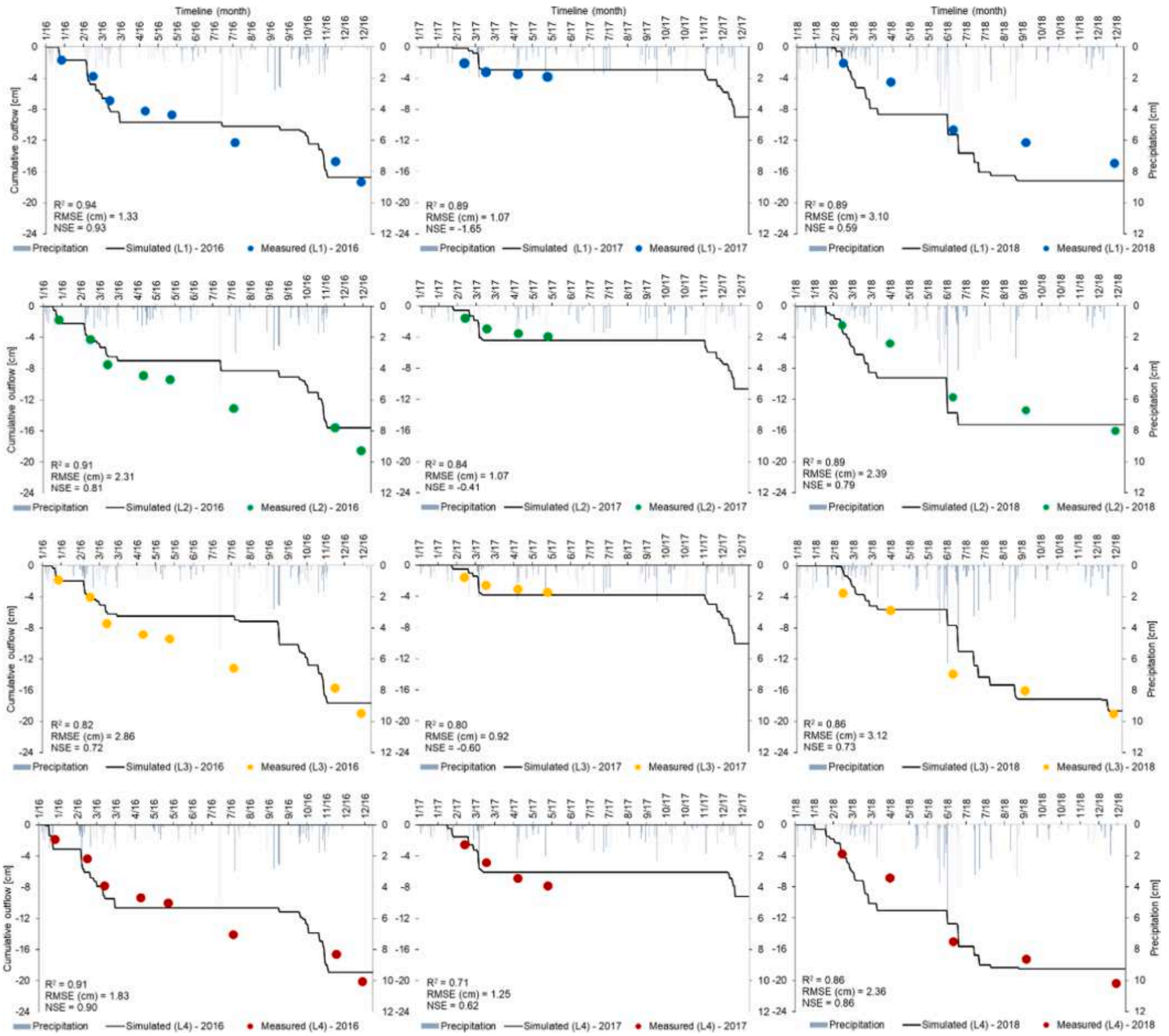

Fig. 2. Measured and simulated cumulative values of leachate from zero-tension lysimeters (L1 - L4), presented with statistical indicators measuring the accuracy (R^2, RMSE, and NSE), installed at Biđ experimental field (Eastern Croatia), using HYDRUS-1D during 2016–2018 (SIM1).

3.2. Autocorrelation analysis

Fig. 3 shows the autocorrelation plots for the precipitation, Sava River, and GW levels. The autocorrelation of the precipitation drops to zero, and remains within the limits of the confidence intervals except in a few cases. The randomness of the correlogram indicates that the precipitation time series mainly consists of short uncorrelated rainfall events. However, there is an overall decreasing trend in the autocorrelation, which suggests a certain precipitation pattern. In particular, the precipitation frequency is higher during the first months and tends to decrease throughout the remaining period, except for the last year where there is again an increase.

On the other hand, the GW and river levels, both exhibit entirely different behaviour. The correlogram of the piezometric level shows a high correlation and a marked seasonality. In particular, the autocorrelation reaches the decorrelation threshold after approximately 80 days, thus suggesting a significant "memory" effect. This behaviour can be related to the high storage capacity of the aquifer, as well as to the hydraulic characteristics of the catchment. The estimated low values of the saturated hydraulic conductivity, K_s, (Table 2) and of the air-entry pressure parameter, α, are correlated with low water flow velocity and high retention capacity, respectively. While being most representative of the unsaturated zone, these parameters could also describe to some extent the hydraulic functioning of the catchment and thus could partially explain the high autocorrelation in the groundwater level time series.

The seasonality effect is less exacerbated in the correlogram of the Sava River level, which reaches the decorrelation threshold after approximately 45 days. The more rapid decorrelation rate is mainly explained by the effect of the direct runoff, while the underlining seasonal effect is induced by the groundwater-river interaction. However, the overall lower autocorrelation compared to the GW level suggests that direct runoff plays a significant role in the river flow dynamics. A similar study, performed in Central Italy, where long-term data (rainfall, river level and groundwater table level) were used to identify surface water-groundwater relationship following the autocorrelation and cross-correlation analyses, pointed out how stationary behaviours were higher for groundwater and surface-water levels than for rainfall, as well

Table 2
Optimized parameters (SCE algorithm) used for numerical simulations (SIM1, SIM2 and SIM3) and parameters obtained by laboratory methods (θ_s, K_s) for soil at selected locations (L1 - L4) at Bid experimental field (eastern Croatia).

	Depth (cm)	θ_s (cm^3 cm^{-3})	θ_r (cm^3 cm^{-3})	K_s (cm day^{-1})	α (cm^{-1})	n (-)
L1	0–40	0.38	0.16	11.0	0.0029	1.43
	40–75	0.37	0.16	15.0	0.0022	1.49
	75–105	0.47	0.09	12.2	0.0080	1.51
	105–200	0.47	0.08	10.6	0.0068	1.57
L2	0–30	0.36	0.15	17.0	0.0018	2.02
	30–75	0.40	0.06	12.0	0.0011	1.16
	75–130	0.46	0.08	13.7	0.0058	1.62
	130–200	0.45	0.07	16.4	0.0050	1.65
L3	0–25	0.43	0.09	12.0	0.0015	1.16
	25–80	0.41	0.16	10.0	0.0039	1.43
	80–110	0.47	0.09	12.2	0.0080	1.51
	110–200	0.47	0.08	10.6	0.0068	1.57
L4	0–30	0.42	0.00	12.0	0.0014	1.20
	30–70	0.41	0.00	14.0	0.0026	1.17
	70–150	0.51	0.10	12.8	0.0121	1.41
	150–200	0.51	0.10	12.8	0.0121	1.41

as a strong pressure transfer from the river to groundwater table (Chiaudani et al., 2017).

3.3. Mutual Information

The estimated MIs between the simulated pressure head and water content, and the main hydrological features, for each lysimeter location, are shown in Figs. 4 and 5. At first inspection, it is evident how the values of the MI are significantly lower for the simulated water content in comparison to the simulated pressure head. In particular, they oscillate between a minimum and a maximum of 0.03 at L3 and 0.25 at L1, respectively. Such low values are mainly explained by the small range of variation in the simulated water content observed at lysimeter locations, which are smoothed by the optimal bin width. On the other hand, the water content oscillations are more appreciable at L1 especially towards the end of the simulation period, thus leading to more appreciable MI values. This diverse behaviour is mainly due to the difference in the estimated van Genuchten-Mualem shape parameters, α, and n, which are higher at particular layers, thus indicating a faster drying out of the porous medium. These parameters in van Genuchten model can have a large influence on soil water dynamics, e.g., there can be a large influence of the n parameter (e.g., Wesseling, Kroes, Campos Oliveira, & Damiano, 2020). A small difference in the shape of the soil water retention curve can lead to substantially different simulation results for fine-textured soils, especially when n parameter is close to 1.0. The

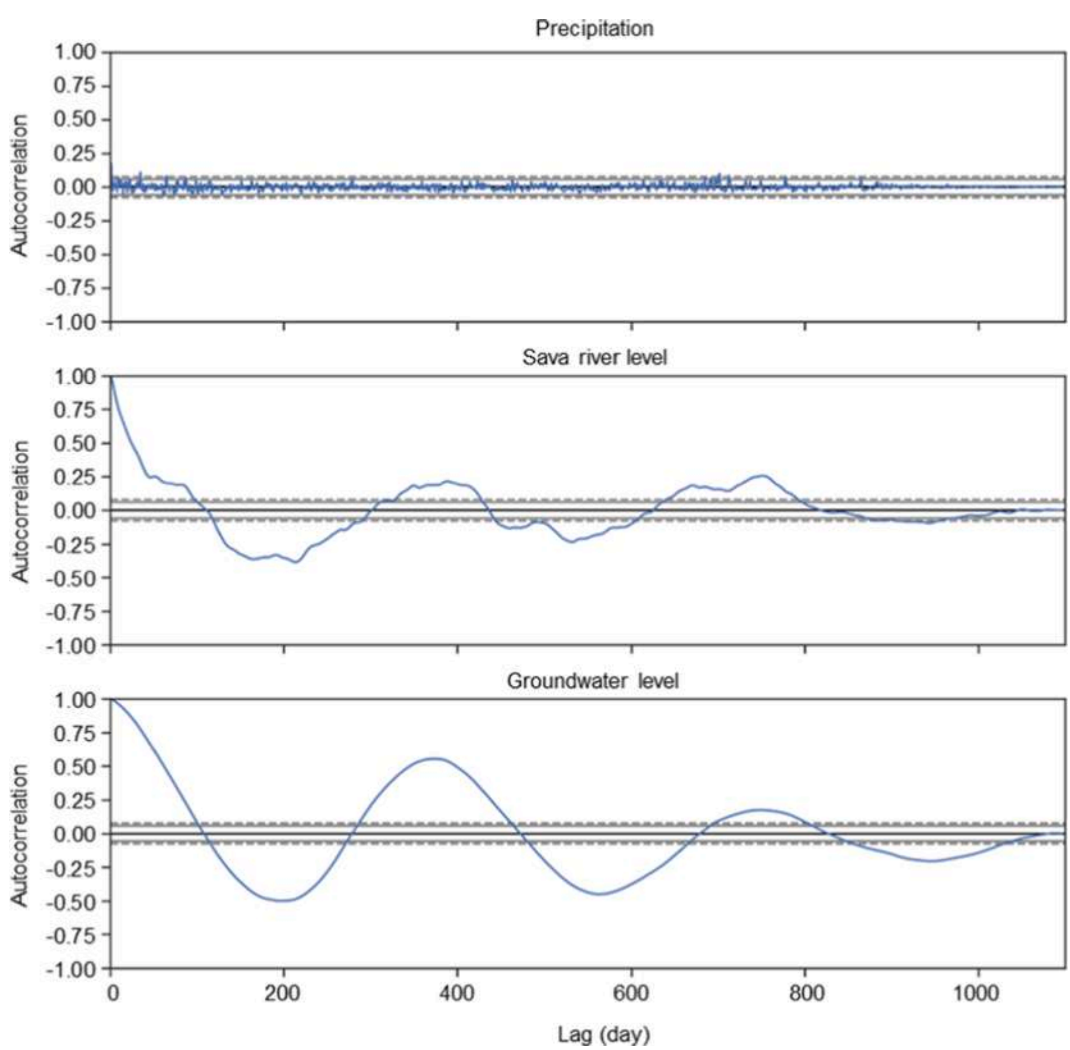

Fig. 3. Autocorrelation plots of the precipitation, Sava River and groundwater levels. The solid and dashed grey lines indicate the 95% and 99% confidence intervals, respectively.

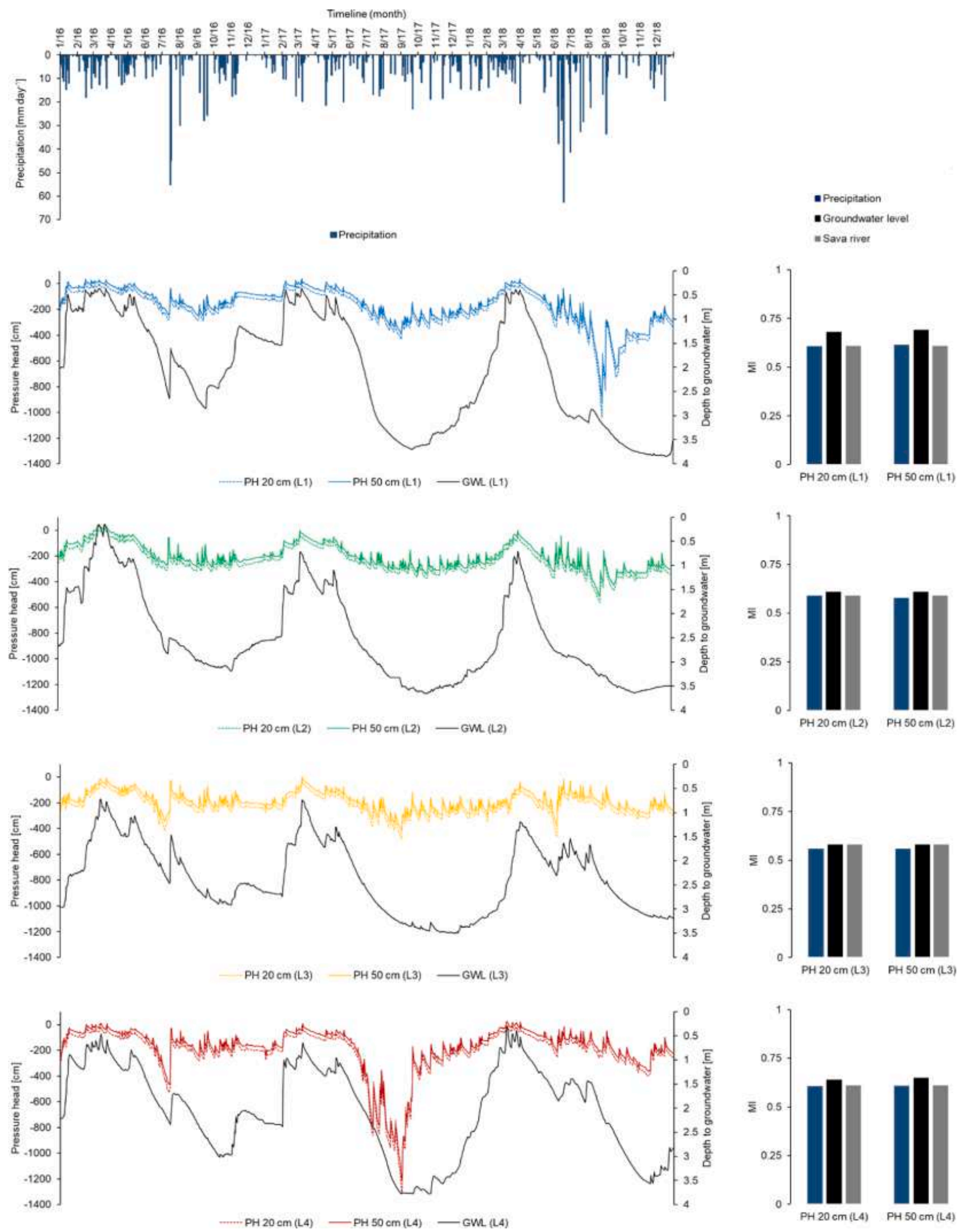

Fig. 4. Pressure head (PH) values simulated with HYDRUS-1D (SIM2) at soil depths of 20 and 50 cm, precipitation, and depths to groundwater (GWL) at locations L1 − 4 at Biđ experimental field (eastern Croatia) during 2016–2018; presented with Mutual Information (MI) values between the PH and precipitation, GW and Sava River levels.

analysis of the estimated MI indicates that the precipitation plays an important role in the simulated water content dynamics, though the difference with the GW and river level is generally not meaningful. Nevertheless, it appears difficult to draw any strong conclusion by considering the combined effect of the optimal bin width and soil hydraulic parameters uncertainty on the estimated MI.

The situation is different when considering the simulated pressure head. In this circumstance, the estimated MI ranges between a minimum and a maximum of 0.56 at L3 and 0.69 at L1, respectively. This is mainly due to the high variations in the simulated pressure head, which provide more information content for the analysis. The precipitation, the GW, and the river level lead to comparable MI values, thus suggesting a concurrent role in the unsaturated flow dynamics. The negligible difference between the locations and depths indicates a homogeneous hydrological behaviour of the experimental area, which appears to be influenced by the GW-river interaction.

3.4. Water storage change

For the observation period of 2016–2018, monthly values of water storage change (*WSC*), cumulative evaporation from the soil surface (*E*), cumulative infiltration into the soil surface (*I*), cumulative root water uptake (plant transpiration) (*T*) and cumulative flux across the bottom boundary (*BF*) are quantified in Table 3 (2016 – 2018) using SIM2 as the

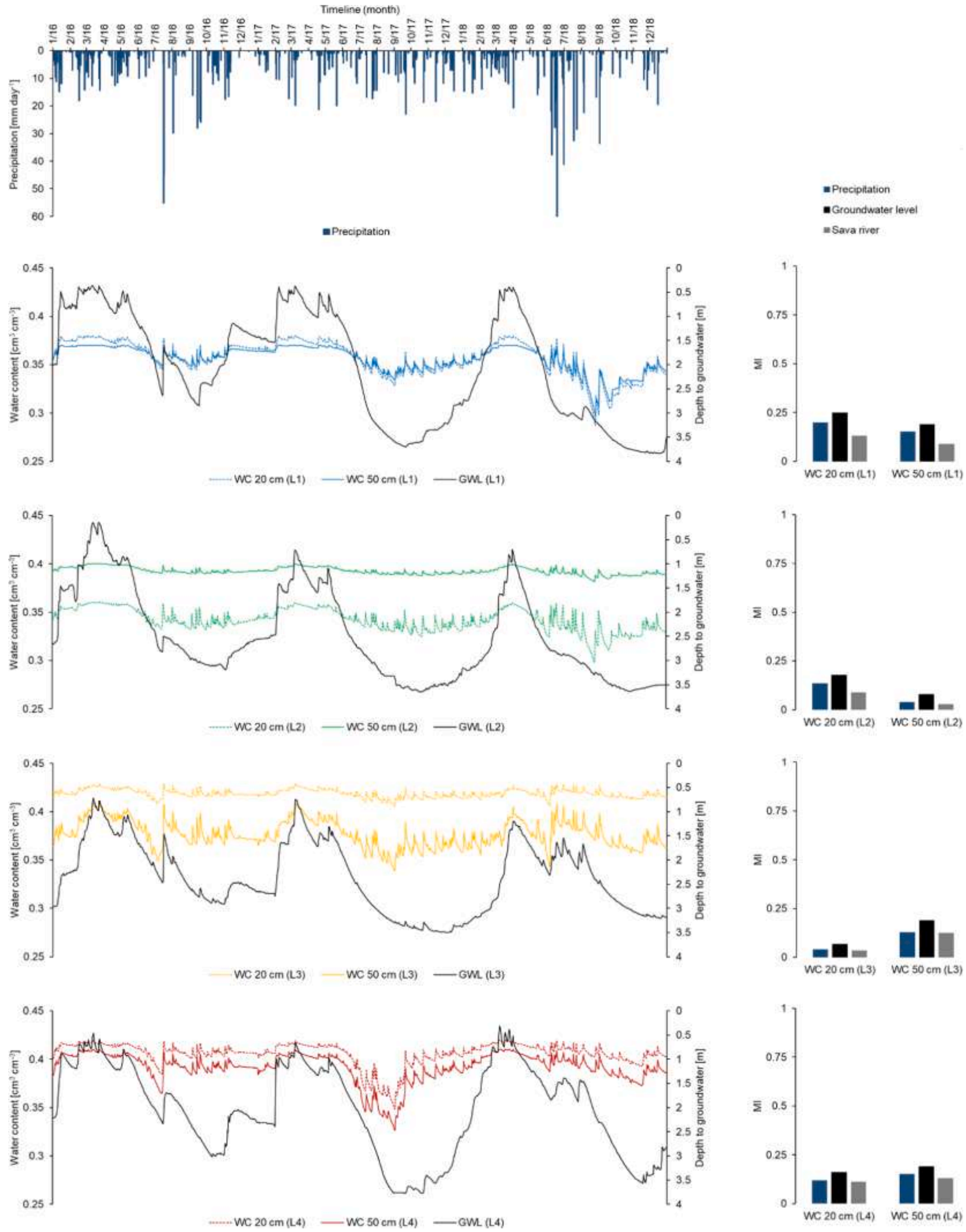

Fig. 5. Water content (WC) simulated with HYDRUS-1D (SIM2) at soil depths of 20 and 50 cm, precipitation, and depths to groundwater (GWL) at locations L1 - L4 at Biđ experimental field (eastern Croatia) during 2016–2018; presented with Mutual Information (MI) values between WC and precipitation, GW and Sava River levels.

best representation of the water balance of the locations. Cumulative transpiration in the investigated period and locations averaged at 38.18 cm. Transpiration differed within locations and years, with the lowest transpiration (16.84 cm) at L2 in soybean (Glycine max L.) in 2017, while the highest was calculated at L3 in 2016 with rapeseed (*Brassica napus L.*) that held the highest value of LAI (5). In addition to the connection with LAI, this variability is connected to the presence of different crops and a different length of the growing season at the corresponding location. Evaporation was less variable among the observed locations, which agrees well with findings from Schneider et al., 2021, who found that evaporation did not vary much, even between different soils. The observation from Merlin et al. (2016) and Tolk, Evett and Schwartz (2015) showed that evaporation rates were affected by differences in soil textures. As in our site the differences in soil properties were small, this also resulted in similar leaching patterns. Positive upward flux into the domain (BF) at all locations peak with the crop harvest, while negative flux is at its highest during the non-growing season when soil remained bare. This suggests a strong connection between the upward direct water fluxes and the root water uptake, as can be seen in Fig. 6. Our results agreed well with previous investigations that showed GW substantially contributed water to plant transpiration and emphasized the importance of water-vegetation interactions in GW-dependent ecosystems (e.g., Barbeta & Peñuelas, 2017; Orellana, Verma, Loheide, & Daly, 2012). Periods where the actual evapotranspiration was directly dependent on GW are highlighted in Fig. 6 by a comparison of simulations that include GW influence (SIM2) to the

Table 3
Water storage change (WSC), cumulative evaporation from the soil surface (E), cumulative infiltration into the soil surface (I), cumulative root water uptake (transpiration, T) and cumulative net flux across the bottom boundary (BF, -/+; out of the domain/into the domain) calculated for L1 – L4 at Bid experimental field, eastern Croatia for 2016–2018.

			Jan.	Feb.	Mar.	Apr.	May	June	July	Aug.	Sep.	Oct.	Nov.	Dec.
	L1	E (cm)	1.00	2.76	5.10	9.15	12.78	19.02	26.32	32.00	36.71	38.95	40.82	41.94
2016	**(OAT)**	T (cm)	0.70	1.94	3.94	10.57	22.18	32.39	33.12	33.12	33.12	33.12	33.12	33.12
		I (cm)	7.10	14.22	21.32	27.08	30.74	35.11	46.31	51.42	60.95	67.54	74.47	74.69
		BF (cm)	2.50	−1.44	−4.36	0.86	11.21	18.92	15.63	10.91	7.92	7.09	6.71	6.86
		WSC (cm)	**7.90**	**8.08**	**7.92**	**8.22**	**6.98**	**2.61**	**2.50**	**−2.79**	**−0.97**	**2.56**	**7.23**	**6.49**
	L2	E (cm)	1.04	2.84	4.90	8.43	12.53	18.84	26.32	32.14	36.98	39.25	41.14	42.27
	(SPELT)	T (cm)	0.95	3.41	6.84	16.64	28.61	39.11	40.08	40.08	40.08	40.08	40.08	40.12
		I (cm)	7.10	14.22	20.98	26.74	30.30	34.67	45.87	50.98	60.51	67.10	74.03	74.69
		BF (cm)	2.08	0.29	−1.17	6.86	17.41	25.19	21.60	19.91	14.16	9.98	7.30	9.73
		WSC (cm)	**7.19**	**8.26**	**8.07**	**8.53**	**6.57**	**1.91**	**1.06**	**−1.34**	**−2.40**	**−2.26**	**0.10**	**2.03**
	L3	E (cm)	0.87	2.23	3.64	5.76	7.62	11.16	16.85	21.40	24.95	26.71	28.15	29.02
	(RAPESEED)	T (cm)	1.37	4.66	9.61	20.90	35.88	51.91	54.90	54.90	54.90	54.90	54.90	54.90
		I (cm)	7.10	14.22	21.32	27.08	30.74	35.11	46.31	51.42	60.95	67.54	74.47	74.69
		BF (cm)	0.62	4.72	5.07	11.88	22.93	33.22	33.64	28.66	21.38	15.99	13.55	12.73
		WSC (cm)	**5.48**	**12.05**	**13.14**	**12.31**	**10.16**	**5.26**	**8.20**	**3.78**	**2.48**	**1.92**	**4.96**	**3.50**
	L4	E (cm)	0.95	2.72	5.06	9.43	14.29	20.54	27.94	33.69	38.37	40.48	42.17	43.16
	(BARLEY)	T (cm)	0.49	1.73	3.85	9.09	16.67	24.90	26.80	26.80	26.80	26.80	26.80	26.80
		I (cm)	7.10	14.22	21.32	27.08	30.74	35.11	46.31	51.42	60.95	67.54	74.47	74.69
		BF (cm)	10.58	7.29	4.37	7.57	14.75	17.19	20.17	14.79	7.29	2.00	3.20	1.62
		WSC (cm)	**16.25**	**17.06**	**16.78**	**16.13**	**14.53**	**6.86**	**11.74**	**5.72**	**3.07**	**2.27**	**8.71**	**6.34**
	L1	E (cm)	0.47	1.48	2.99	4.60	6.74	11.96	18.33	24.02	27.10	29.49	30.85	31.92
2017	**(RAPESEED)**	T (cm)	0.75	3.32	8.02	16.50	30.60	42.03	42.03	42.03	42.03	42.03	42.03	42.03
		I (cm)	2.80	7.40	11.86	18.63	22.94	27.09	34.25	35.90	43.28	49.14	53.42	58.14
		BF (cm)	−2.18	−0.94	0.38	3.85	14.63	21.53	14.53	12.34	10.29	8.21	6.41	4.49
		WSC (cm)	**−0.60**	**1.67**	**1.23**	**1.37**	**0.23**	**−5.37**	**−11.58**	**−17.81**	**−15.56**	**−14.16**	**−13.05**	**−11.31**
	L2	E (cm)	0.63	2.13	5.10	9.05	14.60	20.74	26.12	30.09	32.97	36.16	38.01	39.51
	(SOYBEAN)	T (cm)	0.53	1.79	3.87	7.07	14.17	16.75	16.75	16.75	16.75	16.75	16.75	16.84
		I (cm)	2.80	7.40	11.86	18.63	22.94	27.09	34.25	35.90	43.28	49.14	53.42	58.14
		BF (cm)	−1.37	2.97	3.78	4.06	8.34	8.94	6.19	4.93	−0.67	−3.04	−4.64	−7.59
		WSC (cm)	**0.26**	**6.46**	**6.67**	**6.56**	**2.51**	**−1.45**	**−2.43**	**−6.01**	**−7.10**	**−6.80**	**−5.97**	**−5.80**
	L3	E (cm)	0.60	2.14	5.07	8.84	14.36	21.80	29.96	37.33	41.30	44.17	45.76	47.00
	(BARLEY)	T (cm)	0.32	1.52	4.69	10.00	17.47	18.98	18.98	18.98	18.98	18.98	18.98	19.02
		I (cm)	2.80	7.40	11.86	18.63	22.94	27.09	34.25	35.90	43.28	49.14	53.42	58.14
		BF (cm)	0.07	8.10	9.61	11.89	16.75	16.77	15.91	15.82	14.67	12.09	8.97	4.96
		WSC (cm)	**1.95**	**11.83**	**11.70**	**11.68**	**7.87**	**3.08**	**1.22**	**−4.59**	**−2.33**	**−1.93**	**−2.35**	**−2.92**
	L4	E (cm)	0.62	2.10	5.02	8.69	13.33	18.23	22.39	27.14	30.72	33.44	34.97	36.16
	(SUGARBEET)	T (cm)	0.00	0.00	0.74	3.95	13.14	27.20	38.25	41.96	42.00	42.00	42.00	42.00
		I (cm)	2.80	7.40	11.86	18.63	22.94	27.09	34.25	35.90	43.28	49.14	53.42	58.14
		BF (cm)	3.24	11.39	10.05	10.24	17.15	22.77	24.27	23.51	25.03	25.60	24.22	23.73
		WSC (cm)	**5.41**	**16.69**	**16.15**	**16.23**	**13.62**	**4.42**	**−2.12**	**−9.69**	**−4.41**	**−0.70**	**0.67**	**18.06**
	L1	E (cm)	1.06	1.89	3.85	9.39	16.04	20.93	25.13	28.58	31.56	35.30	36.70	37.61
2018	**(SOYBEAN)**	T (cm)	0.00	0.00	0.00	0.00	4.92	12.27	24.02	38.51	45.30	45.30	45.30	45.30
		I (cm)	6.17	12.76	20.45	23.34	28.78	54.52	63.33	68.73	74.72	77.12	81.27	85.28
		BF (cm)	0.46	1.56	−3.64	−2.08	−4.77	−17.43	−18.54	−10.04	−5.49	−3.27	−2.34	−6.15
		WSC (cm)	**5.56**	**12.43**	**12.97**	**11.87**	**3.05**	**3.89**	**−4.36**	**−8.39**	**−7.63**	**−6.74**	**−3.06**	**−3.78**
	L2	E (cm)	1.08	1.91	3.87	9.43	15.68	20.19	24.10	27.40	31.19	34.92	36.32	37.24
	(SOYBEAN)	T (cm)	0.00	0.00	0.00	1.41	9.33	18.70	31.50	46.86	52.63	52.63	52.63	52.63
		I (cm)	6.17	12.76	20.45	23.34	28.78	54.52	63.33	68.73	74.72	77.12	81.27	85.28
		BF (cm)	−3.27	−3.78	−3.53	−2.78	−0.71	−8.51	−7.56	4.46	8.30	9.14	8.63	4.50
		WSC (cm)	**1.82**	**7.07**	**13.05**	**9.72**	**3.07**	**7.11**	**0.17**	**−1.07**	**−0.80**	**−1.29**	**0.95**	**−0.09**
	L3	E (cm)	0.95	1.56	2.56	4.51	7.97	12.34	17.43	22.93	26.69	30.00	31.23	32.07
	(RAPESEED)	T (cm)	1.53	3.23	8.35	23.75	40.64	46.67	46.67	46.67	46.67	46.67	46.67	46.67
		I (cm)	6.17	12.76	20.45	23.34	28.78	54.52	63.33	68.73	74.72	77.12	81.27	85.28
		BF (cm)	−2.42	−3.24	5.20	16.73	26.50	20.54	11.48	7.85	2.32	1.21	0.15	−5.22
		WSC (cm)	**1.26**	**4.73**	**14.74**	**11.81**	**6.67**	**16.06**	**10.72**	**6.98**	**3.68**	**1.67**	**3.52**	**1.32**
	L4 (SUNFLOWER)	E (cm)	1.01	1.78	3.64	8.83	14.60	18.81	22.65	28.64	33.08	36.91	38.34	39.27
		T (cm)	0.00	0.00	0.00	3.63	11.66	20.62	32.55	38.79	38.79	38.79	38.79	38.79
		I (cm)	6.17	12.76	20.45	23.34	28.78	54.52	63.33	68.73	74.72	77.12	81.27	85.28
		BF (cm)	4.40	3.52	2.23	2.22	6.14	0.95	2.59	3.00	3.86	6.52	6.72	8.12
		WSC (cm)	**9.57**	**14.49**	**19.04**	**13.10**	**8.65**	**16.04**	**10.72**	**4.31**	**6.70**	**7.94**	**10.85**	**15.34**

simulations that excluded GW (SIM3). These events mainly occur during mid to late stage of the growing season, depending on the year and crop, and suggest possible implications with yield performance, as even moderate stresses adversely affect the yield if they occur during crucial stages as flowering (Farooq et al., 2014). The upward-direct net water fluxes during spring/summer prevents further decline of WSC at the corresponding locations, which might be especially important during droughts as it mitigates water stress and reduces the impact of extreme weather conditions on the soil water fluxes (Groh et al., 2020).

4. Conclusions

This study focusing on vadose zone hydrology was performed in gley soils in Eastern Croatia by combining laboratory measurements (soil physical and soil hydraulic parameters i.e., SHP), field observations (lysimeters, crop parameters, groundwater table and river level) and numerical modeling using HYDRUS-1D. The seasonal water regime dynamics was described using the SHP optimized with Shuffled Complex Evolution (SCE) algorithm. The measured lysimeter outflow data was

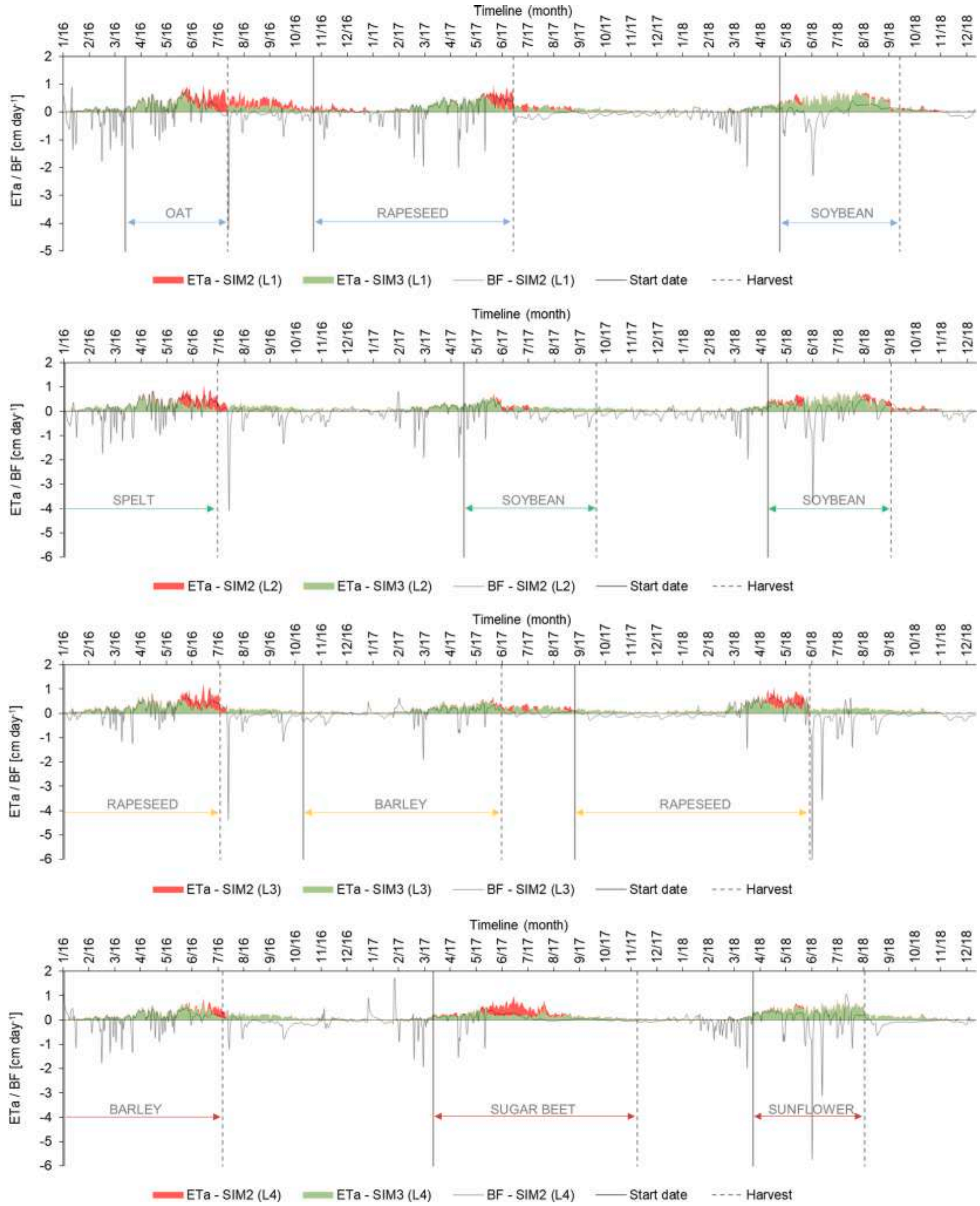

Fig. 6. Bottom flux (BF) at 2 m depth (positive upward flux – inflow and negative leaching – outflow from the domain), actual evapotranspiration (ETa) simulated with groundwater (SIM2) and actual evapotranspiration (ETa) simulated with free drainage as the lower boundary condition (SIM3) (cm day^{-1}) values at locations L1 - L4 at Biđ experimental field (eastern Croatia), during 2016 – 2018.

successfully reproduced (R^2 0.72 – 0.94) and zero-tension lysimeters displayed their feasibility as a measurement system to provide data on soil water fluxes for model validation. The lysimeter outflows were connected to precipitation patterns, transpiration intensity and soil moisture state which was influenced by the shallow water table. The low amount of precipitation during the observed year accentuated the effect of groundwater level on soil water in the root zone. The results demonstrate that the climate variability, seasonally elevated groundwater level, and groundwater-river interaction can significantly influence the fine textured soil pressure head (PH) and water content (WC). The precipitation, groundwater, and river level data had comparable Mutual Information (MI) values, thus suggested their concurrent role in the unsaturated flow dynamics. The negligible difference between the locations and groundwater depths suggests homogeneous hydrological behaviour of the experimental area, which appears to be influenced by the groundwater river interaction. The relationship between upward flux/water storage change into the domain and transpiration/growth stages suggest a strong connection between the fluxes and the root water uptake. Groundwater considerably contributed to plant transpiration and pointed out the importance of water-vegetation interactions in groundwater-dependent ecosystems. The upward-directed net water fluxes during spring/summer prevents further decline in water storage change at the study locations, which might be crucial for reducing the impact of extreme weather conditions on soil water fluxes and for alleviating water stress during droughts. While evaporation was less variable among the observed locations, transpiration differed within locations, due to the presence of different crops and duration of the growing season and its connection with crop and site-specific LAI. The vadose zone soil appears to be sensitive to the complex hydrological interactions between its boundaries, especially in agricultural areas with shallow groundwater table. Long term field data combined with appropriate statistical and numerical tools can give more insight into the surface–groundwater interaction.

Declaration of Competing Interest

The authors declare that they have no known competing financial interests or personal relationships that could have appeared to influence the work reported in this paper.

Acknowledgments

Financial support for this research was provided through the project "Monitoring the water regime and water quality of agricultural soils in the ameliorative irrigation canal in Biđ-Bosut field" by Croatian Waters.

Appendix A. Supplementary material

Supplementary data to this article can be found online at https://doi.org/10.1016/j.catena.2021.105987.

References

Adhikari, K., Hartemink, A.E., 2016. Linking soils to ecosystem services - A global review. Geoderma 262, 101–111. https://doi.org/10.1016/j.geoderma.2015.08.009.

Allen, R.G., Pereira, L.S., Raes, D., Smith, M., 1998. FAO Irrigation and Drainage Paper No. 56 - Crop Evapotranspiration.

Askri, B., Ahmed, A.T., Abichou, T., Bouhlila, R., 2014. Effects of shallow water table, salinity and frequency of irrigation water on the date palm water use. J. Hydrol. 513, 81–90. https://doi.org/10.1016/j.jhydrol.2014.03.030.

Ayars, J.E., Christen, E.W., Soppe, R.W., Meyer, W.S., 2006. The resource potential of in-situ shallow ground water use in irrigated agriculture: A review. Irrig. Sci. 24 (3), 147–160. https://doi.org/10.1007/s00271-005-0003-y.

Bailey, R.T., Wible, T.C., Arabi, M., Records, R.M., Ditty, J., 2016. Assessing regional-scale spatio-temporal patterns of groundwater–surface water interactions using a coupled SWAT-MODFLOW model. Hydrol. Process. 30, 4420–4433. https://doi.org/10.1002/hyp.10933.

Barbeta, A., Peñuelas, J., 2017. Relative contribution of groundwater to plant transpiration estimated with stable isotopes. Sci Rep 7 (1). https://doi.org/10.1038/s41598-017-09643-x.

Bethune, M.G., Selle, B., Wang, Q.J., 2008. Understanding and predicting deep percolation under surface irrigation. Water Resour. Res. 44, 1–16. https://doi.org/10.1029/2007WR006380.

Breuer, L., Eckhardt, K., Frede, H.-G., 2003. Plant parameter values for models in temperate climates. Ecol. Modell. 169 (2-3), 237–293. https://doi.org/10.1016/S0304-3800(03)00274-6.

Cao, R., Jia, X., Huang, L., Zhu, Y., Wu, L., Shao, M., 2018. Deep soil water storage varies with vegetation type and rainfall amount in the Loess Plateau of China. Sci. Rep. 8, 1–12. https://doi.org/10.1038/s41598-018-30850-7.

Chapman, T.G., 1986. Entropy as a measure of hydrologic data uncertainty and model performance. J. Hydrol. 85 (1-2), 111–126. https://doi.org/10.1016/0022-1694(86)90079-X.

Chen, X.i., Hu, Q.i., 2004. Groundwater influences on soil moisture and surface evaporation. J. Hydrol. 297 (1-4), 285–300. https://doi.org/10.1016/j.jhydrol.2004.04.019.

Chiaudani, A., Di Curzio, D., Palmucci, W., Pasculli, A., Polemio, M., Rusi, S., 2017. Statistical and fractal approaches on long time-series to surface-water/groundwater relationship assessment: A central Italy alluvial plain case study. Water 9, 850. https://doi.org/10.3390/w9110850.

Coquet, Y., Coutadeur, C., Labat, C., Vachier, P., van Genuchten, M.T., Roger-Estrade, J., Šimůnek, J., 2005. Water and Solute Transport in a Cultivated Silt Loam Soil: 1 Field Observations. Vadose Zo. J. 4 (3), 573–586. https://doi.org/10.2136/vzj2004.0152.

Dane, J.H., Hopmans, J.W., 2002. Methods of Soil Analysis: Water Retention and Storage. In: Dane, H.J., Topp, C.G. (Eds.), Methods of Soil Analysis. SSSA Book Series, Madison, WI, pp. 671–673. https://doi.org/10.2136/sssabookser5.4.c24.

Dettmann, U., 2020. SoilHyP: Soil Hydraulic Properties. R package version (1), 4.

Duan, Q.Y., Gupta, V.K., Sorooshian, S., 1993. Shuffled Complex Evolution Approach for Effective and Efficient Global Minimization. J. Optim. Theory Appl. 76 (3), 501–521. https://doi.org/10.1007/BF00939380.

Fan, Y., 2015. Groundwater in the Earth's critical zone: Relevance to large-scale patterns and processes. Water Resour. Res. 51 (5), 3052–3069. https://doi.org/10.1002/2015WR017037.

Fan, Y., Li, H., Miguez-Macho, G., 2013. Global patterns of groundwater table depth. Science (80-). 339 (6122), 940–943.

Farooq, M., Hussain, M., Siddique, K.H.M., 2014. Drought Stress in Wheat during Flowering and Grain-filling Periods. CRC. Crit. Rev. Plant Sci. 33 (4), 331–349. https://doi.org/10.1080/07352689.2014.875291.

Feddes, R.A., Kowalik, P.J., Zaradny, H., 1978. Simulation of Field Water Use and Crop Yield. John Wiley & Sons, New York.

Filipović, V., Coquet, Y., Pot, V., Houot, S., Benoit, P., 2016. Modeling water and isoproturon dynamics in a heterogeneous soil profile under different urban waste compost applications. Geoderma 268, 29–40. https://doi.org/10.1016/j.geoderma.2016.01.009.

Filipović, V., Coquet, Y., Pot, V., Houot, S., Benoit, P., 2014. Modeling the effect of soil structure on water flow and isoproturon dynamics in an agricultural field receiving repeated urban waste compost application. Sci. Total Environ. 499, 546–559. https://doi.org/10.1016/j.scitotenv.2014.06.010.

Filipović, V., Kodešová, R., Petošić, D., 2013. Experimental and mathematical modeling of water regime and nitrate dynamics on zero tension plate lysimeters in soil influenced by high groundwater table. Nutr. Cycl. Agroecosyst. 95 (1), 23–42. https://doi.org/10.1007/s10705-012-9546-5.

Fischer, E.M., Knutti, R., 2014. Detection of spatially aggregated changes in temperature and precipitation extremes. Geophys. Res. Lett. 41 (2), 547–554. https://doi.org/10.1002/2013GL058499.

Gee, G.W., Or, D., 2002. Methods of Soil Analysis: Particle-size analysis, in: Dane, J.H., Topp, G.C. (Eds.), Methods of Soil Analysis. Madison, WI, pp. 1381–1402. https://doi.org/10.2136/sssabookser5.4.c12.

Gentle, J.E., Härdle, W.K., Mori, Y., 2012. Handbook of Computational Statistics. Springer. https://doi.org/10.1007/978-3-642-21551-3.

Gogolev, M.I., 2002. Assessing groundwater recharge with two unsaturated zone modeling technologies. Environ. Geol. 42 (2-3), 248–258. https://doi.org/10.1007/s00254-001-0494-7.

Gong, W., Yang, D., Gupta, H.V., Nearing, G., 2014. Estimating information entropy for hydrological data: One-dimensional case. Water Resour. Res. 50 (6), 5003–5018. https://doi.org/10.1002/2014WR015874.

Green, T.R., 2016. In: Integrated Groundwater Management. Springer International Publishing, Cham, pp. 97–141. https://doi.org/10.1007/978-3-319-23576-9_5.

Gribovszki, Z., Szilágyi, J., Kalicz, P., 2010. Diurnal fluctuations in shallow groundwater levels and streamflow rates and their interpretation - A review. J. Hydrol. 385 (1-4), 371–383. https://doi.org/10.1016/j.jhydrol.2010.02.001.

Grimaldi, S., Orellana, F., Daly, E., 2015. Modelling the effects of soil type and root distribution on shallow groundwater resources. Hydrol. Process. 29 (20), 4457–4469. https://doi.org/10.1002/hyp.10503.

Groh, J., Stumpp, C., Lücke, A., Pütz, T., Vanderborght, J., Vereecken, H., 2018. Inverse Estimation of Soil Hydraulic and Transport Parameters of Layered Soils from Water Stable Isotope and Lysimeter Data. Vadose Zo. J. 17 (1), 170168. https://doi.org/10.2136/vzj2017.09.0168.

Groh, J., Vanderborght, J., Pütz, T., Vereecken, H., 2016. How to Control the Lysimeter Bottom Boundary to Investigate the Effect of Climate Change on Soil Processes? Vadose Zo. J. 15. https://doi.org/10.2136/vzj2015.08.0113.

Groh, J., Vanderborght, J., Pütz, T., Vogel, H.-J., Gründling, R., Rupp, H., Rahmati, M., Sommer, M., Vereecken, H., Gerke, H.H., 2020. Responses of soil water storage and crop water use efficiency to changing climatic conditions: A lysimeter-based space-for-time approach. Hydrol. Earth Syst. Sci. 24 (3), 1211–1225. https://doi.org/10.5194/hess-24-1211-2020.

Han, M., Zhao, C., Šimůnek, J., Feng, G., 2015. Evaluating the impact of groundwater on cotton growth and root zone water balance using Hydrus-1D coupled with a crop growth model. Agric. Water Manag. 160, 64–75. https://doi.org/10.1016/j.agwat.2015.06.028.

IUSS, 2015. International soil classification system for naming soils and creating legends for soil maps: World reference base for soil resources 2014 (Update 2015), in: World Soil Resources Reports No. 106. FAO, Rome, Italy, p. 192.

Jiménez-Martínez, J., Skaggs, T.H., van Genuchten, M.T., Candela, L., 2009. A root zone modelling approach to estimating groundwater recharge from irrigated areas. J. Hydrol. 367 (1-2), 138–149. https://doi.org/10.1016/j.jhydrol.2009.01.002.

Karimov, A.K., Šimůnek, J., Hanjra, M.A., Avliyakulov, M., Forkutsa, I., 2014. Effects of the shallow water table on water use of winter wheat and ecosystem health: Implications for unlocking the potential of groundwater in the Fergana Valley (Central Asia). Agric. Water Manag. 131, 57–69. https://doi.org/10.1016/j.agwat.2013.09.010.

Klammler, G., Fank, J., 2014. Determining water and nitrogen balances for beneficial management practices using lysimeters at Wagna test site (Austria). Sci. Total Environ. 499, 448–462. https://doi.org/10.1016/j.scitotenv.2014.06.009.

Klute, A., Dirksen, C., 1986. Hydraulic Conductivity and Diffusivity: Laboratory Methods. Methods Soil Anal. Part 1—Physical Mineral. Methods 687–734. https://doi.org/10.2136/sssabookser5.1.2ed.c28.

Kollet, S.J., Maxwell, R.M., 2008. Capturing the influence of groundwater dynamics on land surface processes using an integrated, distributed watershed model. Water Resour. Res. 44, 1–18. https://doi.org/10.1029/2007WR006004.

Li, Q., Zipper, S.C., Gleeson, T., 2020. Streamflow depletion from groundwater pumping in contrasting hydrogeological landscapes: Evaluation and sensitivity of a new management tool. J. Hydrol. 590, 125568. https://doi.org/10.1016/j.jhydrol.2020.125568.

Loritz, R., Gupta, H., Jackisch, C., Westhoff, M., Kleidon, A., Ehret, U., Zehe, E., 2018. On the dynamic nature of hydrological similarity. Hydrol. Earth Syst. Sci. 22, 3663–3684. https://doi.org/10.5194/hess-22-3663-2018.

Lu, X., Jin, M., Van Genuchten, M.T., Wang, B., 2011. Groundwater Recharge at Five Representative Sites in the Hebei Plain, China. Ground Water 49, 286–294. https://doi.org/10.1111/j.1745-6584.2009.00667.x.

Martínez-De La Torre, A., Miguez-Macho, G., 2019. Groundwater influence on soil moisture memory and land-atmosphere fluxes in the Iberian Peninsula. Hydrol. Earth Syst. Sci. 23, 4909–4932. https://doi.org/10.5194/hess-23-4909-2019.

Mattern, S., Vanclooster, M., 2010. Estimating travel time of recharge water through a deep vadose zone using a transfer function model. Environ. Fluid Mech. 10 (1-2), 121–135. https://doi.org/10.1007/s10652-009-9148-1.

Mekonnen, M.M., Hoekstra, A.Y., 2016. Sustainability: Four billion people facing severe water scarcity. Sci. Adv. 2, 1–7. https://doi.org/10.1126/sciadv.1500323.

Merlin, O., Stefan, V.G., Amazirh, A., Chanzy, A., Ceschia, E., Er-Raki, S., Gentine, P., Tallec, T., Ezzahar, J., Bircher, S., Beringer, J., Khabba, S., 2016. Modeling soil evaporation efficiency in a range of soil and atmospheric conditions using a meta-analysis approach. Water Resour. Res. 52 (5), 3663–3684. https://doi.org/10.1002/2015WR018233.

Michaels, G.S., Carr, D.B., Askenazi, M., Fuhrman, S., Wen, X., Somogyi, R., 1998. Cluster analysis and data visualization of large-scale gene expression data., in: Pacific Symposium on Biocomputing. pp. 42–53.

Monteith, J.L., 1981. Evaporation and surface temperature. Q. J. R. Meteorol. Soc. 107, 1–27. https://doi.org/10.1256/smsqj.45101.

Moriasi, D.N., Arnold, J.G., Van Liew, M.W., Bingner, R.L., Harmel, R.D., Veith, T.L., 2007. Model evaluation guidelines for systematic quantification of accuracy in watershed simulations. Am. Soc. Agric. Biol. Eng. 50, 885–900. https://doi.org/10.13031/2013.23153.

Mualem, Y., 1976. A new model for predicting the hydraulic conductivity of unsatuated porous media. Water Resour. Res. 12, 513–522. https://doi.org/10.1029/WR012i003p00513.

Nestroy, O., 2008. The importance of unsaturated soil zone for the regional water balance. Ecohydrol. Hydrobiol. 8 (2-4), 385–389. https://doi.org/10.2478/v10104-009-0030-z.

Nosetto, M.D., Jobbágy, E.G., Jackson, R.B., Sznaider, G.A., 2009. Reciprocal influence of crops and shallow ground water in sandy landscapes of the Inland Pampas. F. Crop. Res. 113 (2), 138–148. https://doi.org/10.1016/j.fcr.2009.04.016.

Orellana, F., Verma, P., Loheide, S.P., Daly, E., 2012. Monitoring and modeling water-vegetation interactions in groundwater-dependent ecosystems. Rev. Geophys. 50, 1–24. https://doi.org/10.1029/2011RG000383.

Pütz, T., Fank, J., Flury, M., 2018. Lysimeters in Vadose Zone Research. Vadose Zo. J. 17 (1), 180035. https://doi.org/10.2136/vzj2018.02.0035.

Pütz, T.h., Kiese, R., Wollschläger, U., Groh, J., Rupp, H., Zacharias, S., Priesack, E., Gerke, H.H., Gasche, R., Bens, O., Borg, E., Baessler, C., Kaiser, K., Herbrich, M., Munch, J.-C., Sommer, M., Vogel, H.-J., Vanderborght, J., Vereecken, H., 2016. TERENO-SOILCan: a lysimeter-network in Germany observing soil processes and plant diversity influenced by climate change. Environ. Earth Sci. 75 (18) https://doi.org/10.1007/s12665-016-6031-5.

Ries, F., Lange, J., Schmidt, S., Puhlmann, H., Sauter, M., 2015. Recharge estimation and soil moisture dynamics in a Mediterranean, semi-arid karst region. Hydrol. Earth Syst. Sci. 19, 1439–1456. https://doi.org/10.5194/hess-19-1439-2015.

Robinson, D.A., Hopmans, J.W., Filipovic, V., van der Ploeg, M., Lebron, I., Jones, S.B., Reinsch, S., Jarvis, N., Tuller, M., 2019. Global environmental changes impact soil hydraulic functions through biophysical feedbacks. Glob. Chang. Biol. 25 (6), 1895–1904. https://doi.org/10.1111/gcb.14626.

Safavi, H.R., Darzi, F., Mariño, M.A., 2010. Simulation-Optimization Modeling of Conjunctive Use of Surface Water and Groundwater. Water Resour. Manag. 24 (10), 1965–1988. https://doi.org/10.1007/s11269-009-9533-z.

Schaap, M.G., Leij, F.J., van Genuchten, M.T., 2001. Rosetta: a computer program for estimating soil hydraulic parameters with hierarchical pedotransfer functions. J. Hydrol. 251 (3-4), 163–176. https://doi.org/10.1016/S0022-1694(01)00466-8.

Schneider, J., Groh, J., Pütz, T., Helmig, R., Rothfuss, Y., Vereecken, H., Vanderborght, J., 2021. Prediction of soil evaporation measured with weighable lysimeters using the FAO Penman-Monteith method in combination with Richards' equation. Vadose Zo. J. 20 (1) https://doi.org/10.1002/vzj2.v20.110.1002/vzj2.20102.

Šimůnek, J., Bradford, S.A., 2008. Vadose Zone Modeling: Introduction and Importance. Vadose Zo. J. 7 (2), 581–586. https://doi.org/10.2136/vzj2008.0012.

Šimůnek, J., Genuchten, M.T., Šejna, M., 2016. Recent Developments and Applications of the HYDRUS Computer Software Packages. Vadose Zo. J. 15 (7), 1–25. https://doi.org/10.2136/vzj2016.04.0033.

Soylu, M.E., Istanbulluoglu, E., Lenters, J.D., Wang, T., 2011. Quantifying the impact of groundwater depth on evapotranspiration in a semi-arid grassland region. Hydrol. Earth Syst. Sci. 15, 787–806. https://doi.org/10.5194/hess-15-787-2011.

Stumpp, C., Stichler, W., Kandolf, M., Šimůnek, J., 2012. Effects of Land Cover and Fertilization Method on Water Flow and Solute Transport in Five Lysimeters: A Long-Term Study Using Stable Water Isotopes. Vadose Zo. J. 11 (1) https://doi.org/10.2136/vzj2011.0075.

Tolk, J.A., Evett, S.R., Schwartz, R.C., 2015. Field-Measured, Hourly Soil Water Evaporation Stages in Relation to Reference Evapotranspiration Rate and Soil to Air Temperature Ratio. Vadose Zo. J. 14. https://doi.org/10.2136/vzj2014.07.0079.

van Genuchten, M.T., 1980. A closed-form equation for predicting the hydraulic conductivity of unsaturated soils. Soil Sci. Soc. Am. J. 44 (5), 892–898. https://doi.org/10.2136/sssaj1980.03615995004400050002x.

Ventrella, D., Mohanty, B.P., ??im??nek, J., Losavio, N., van Genuchten, M.T., 2000. Water and chloride transport in a fine-textured soil: Field experiments and modeling. Soil Sci. 165 (8), 624–631. https://doi.org/10.1097/00010694-200008000-00004.

Vereecken, H., Schnepf, A., Hopmans, J.W., Javaux, M., Or, D., Roose, T., Vanderborght, J., Young, M.H., Amelung, W., Aitkenhead, M., Allison, S.D., Assouline, S., Baveye, P., Berli, M., Brüggemann, N., Finke, P., Flury, M., Gaiser, T., Govers, G., Ghezzehei, T., Hallett, P., Hendricks Franssen, H.J., Heppell, J., Horn, R., Huisman, J.A., Jacques, D., Jonard, F., Kollet, S., Lafolie, F., Lamorski, K., Leitner, D., McBratney, A., Minasny, B., Montzka, C., Nowak, W., Pachepsky, Y., Padarian, J., Romano, N., Roth, K., Rothfuss, Y., Rowe, E.C., Schwen, A., Šimůnek, J., Tiktak, A., Van Dam, J., van der Zee, S.E.A.T.M., Vogel, H.J., Vrugt, J.A., Wöhling, T., Young, I.M., 2016. Modeling Soil Processes: Review, Key Challenges, and New Perspectives. Vadose Zo. J. 15, vzj2015.09.0131. https://doi.org/10.2136/vzj2015.09.0131.

Vereecken, H., Weynants, M., Javaux, M., Pachepsky, Y., Schaap, M.G., van Genuchten, M.T., 2010. Using Pedotransfer Functions to Estimate the van Genuchten-Mualem Soil Hydraulic Properties: A Review. Vadose Zo. J. 9 (4), 795–820. https://doi.org/10.2136/vzj2010.0045.

Vöröšmarty, C.J., Green, P., Salisbury, J., Lammers, R.B., 2000. Global water resources: Vulnerability from climate change and population growth. Science (80-). 289 (5477), 284–288.

Vrugt, J.A., Gupta, H.V., Bouten, W., Sorooshian, S., 2003. A Shuffled Complex Evolution Metropolis algorithm for optimization and uncertainty assessment of hydrologic model parameters. Water Resour. Res. 39 (8) https://doi.org/10.1029/2002WR001642.

Wada, Y., Wisser, D., Bierkens, M.F.P., 2014. Global modeling of withdrawal, allocation and consumptive use of surface water and groundwater resources. Earth Syst. Dyn. 5, 15–40. https://doi.org/10.5194/esd-5-15-2014.

Wesseling, J., Kroes, J., Campos Oliveira, T., Damiano, F., 2020. The impact of sensitivity and uncertainty of soil physical parameters on the terms of the water balance: Some case studies with default R packages. Part II: Results and discussion. Comput. Electron. Agric. 170, 105072. https://doi.org/10.1016/j.compag.2019.105072.

Westerhoff, R., White, P., Rawlinson, Z., 2018. Incorporation of satellite data and uncertainty in a nationwide groundwater recharge model in New Zealand. Remote Sens. 10, 1–25. https://doi.org/10.3390/rs10010058.

Winter, T.C., 1999. Relation of streams, lakes, and wetlands to groundwater flow systems. Hydrogeol. J. 7 (1), 28–45. https://doi.org/10.1007/s100400050178.

Wu, Q., Si, B., He, H., Wu, P., 2019. Determining regional-scale groundwater recharge with GRACE and GLDAS. Remote Sens. 11 (2), 154. https://doi.org/10.3390/rs11020154.

Yang, J., Yu, Z., Yi, P., Frape, S.K., Gong, M., Zhang, Y., 2020. Evaluation of surface water and groundwater interactions in the upstream of Kui river and Yunlong lake, Xuzhou China. J. Hydrol. 583, 124549. https://doi.org/10.1016/j.jhydrol.2020.124549.

Yang, Y., Liu, D.L., Anwar, M.R., O'Leary, G., Macadam, I., Yang, Y., 2016. Water use efficiency and crop water balance of rainfed wheat in a semi-arid environment: sensitivity of future changes to projected climate changes and soil type. Theor. Appl. Climatol. 123 (3-4), 565–579. https://doi.org/10.1007/s00704-015-1376-3.

Zhang, X., 2015. Conjunctive surface water and groundwater management under climate change. Front. Environ. Sci. 3, 1–10. https://doi.org/10.3389/fenvs.2015.00059.

Zheng, H., Gao, J., Teng, Y., Feng, C., Tian, M., Li, C., 2015. Temporal variations in soil moisture for three typical vegetation types in inner mongolia, northern china. PLoS One 10 (3), e0118964. https://doi.org/10.1371/journal.pone.0118964.

Zhu, Y., Ren, L., Zhang, Q., Lü, H., Yu, Z., Wu, Y., Feng, H., 2009. The contribution of groundwater to soil moisture in Populus euphratica root zone layer. Ecohydrol. Surf. Groundw. Depend. Syst. Concepts, Methods Recent Dev. 181–188.

Zipper, S.C., Soylu, M.E., Booth, E.G., Loheide, S.P., 2015. Untangling the effects of shallow groundwater and soil texture as drivers of subfield-scale yield variability. Water Resour. Res. 51 (8), 6338–6358. https://doi.org/10.1002/2015WR017522.